Published in final edited form as:
Ann Biomed Eng. 2014 July ; 42(7): 1470–1481. doi:10.1007/s10439-013-0883-6.

Cellularized microcarriers as adhesive building blocks for fabrication of tubular tissue constructs

Waleed O. Twal[1,2], **Sandra C. Klatt**[1,2], **Keerthi Harikrishnan**[1], **Ebtesam Gerges**[1], **Marion A. Cooley**[1], **Thomas C. Trusk**[1], **Boran Zhou**[3], **Mohamed G. Gabr**[3], **Tarek Shazly**[3,4], **Susan M. Lessner**[3,5], **Roger R. Markwald**[1], and **W. Scott Argraves**[1,6]

[1]Department of Regenerative Medicine and Cell Biology, Medical University of South Carolina, Charleston, SC 29425 USA

[3]College of Engineering and Computing, Biomedical Engineering Program, University of South Carolina, Columbia, SC, 29208, USA

[4]College of Engineering and Computing, Mechanical Engineering Department, University of South Carolina, Columbia, SC, 29208, USA

[5]University of South Carolina School of Medicine, Department of Cell Biology and Anatomy, Columbia, SC 29208, USA

Abstract

To meet demands of vascular reconstruction, there is a need for prosthetic alternatives to natural blood vessels. Here we explored a new conduit fabrication approach. Macroporous, gelatin microcarriers laden with human umbilical vein endothelial cells and aortic smooth muscle cells were dispensed into tubular agarose molds and found to adhere to form living tubular tissues. The ability of cellularized microcarriers to adhere to one another involved cellular and extracellular matrix bridging that included the formation of epithelium-like cell layers lining the lumenal and ablumenal surfaces of the constructs and the deposition of collagen and elastin fibers. The tubular tissues behaved as elastic solids, with a uniaxial mechanical response that is qualitatively similar to that of native vascular tissues and consistent with their elastin and collagen composition. Linearized measures of the mechanical response of the fabricated tubular tissues at both low and high strains was observed to increase with duration of static culture, with no significant loss of stiffness following decellularization. The findings highlight the utility of cellularized macroporous gelatin microcarriers as self-adhering building blocks for the fabrication of living tubular structures.

[6]*Address corresponding to*: W. Scott Argraves, Ph.D., Department of Regenerative Medicine and Cell Biology, Medical University of South Carolina, 173 Ashley Avenue, BSB 653, Charleston, SC 29425 USA, argraves@musc.edu.
[2]Equal contribution (co-first author)

Disclosure Statement
No competing financial interests exist.

Introduction

Limitations exist for the availability of suitable autologous vascular conduits derived from a patient body for vascular replacement procedures such as coronary artery bypass grafting [1]. Therefore, there is a need for prosthetic alternatives to autologous vascular conduits. A variety of approaches have been developed to fabricate blood vessels [2–7]. These include the use of tubular scaffolds manufactured from natural and synthetic biomaterials that are subsequently seeded with vascular cells to create living prostheses [7–10]. We were motivated to explore alternative approaches that would facilitate cell-based fabrication of conduits comprised of vascular cells and extracellular matrix (ECM) constituents that they synthesize.

Microcarrier beads are 100–300 μm diameter spherical particles that allow attachment and growth of anchorage-dependent cells while in suspension culture [11–13]. Microcarrier beads are manufactured from natural and synthetic materials, including gelatin, collagen, dextran, glass, polyethylene and polystyrene. Variant forms of microcarrier beads are macroporous, having large pores of tens of micrometers that provide additional areas for cells to attach and grow [14, 15].

Microcarriers have been generally used for suspension tissue culture to produce high yields of anchorage-dependent cells and their secreted products, but in recent years their utility in tissue regeneration and tissue engineering has emerged [16, 17]. For example, microcarriers have been used as cell delivery systems to regenerate tissue at sites of injury [17]. Transplantation of skin cell-containing microcarriers onto cutaneous wounds of rodents and humans has been shown to lead to dermal regeneration [18–21] and a reduction in detrimental wound contraction [22]. Implantation of gelatin microcarriers loaded with bone marrow-derived mesenchymal stem cells has been shown to improve bone regeneration of craniofacial and long bone defects [23, 24]. An additional benefit of the gelatin microcarriers used in such applications is that they degrade over time *in vivo* without eliciting an inflammatory reaction [25, 26].

Only a few studies have explored the use of cellularized microcarriers as building blocks for three-dimensional (3D) tissue fabrication. Small disc-shaped constructs (1–2 cm in diameter × 0.1–0.8 cm in thickness) have been fabricated from dermal fibroblast-containing macroporous gelatin microcarriers [27, 28]. Similarly, cylindrical bone tissue constructs (2 cm in diameter × 1 cm in thickness) have been fabricated from macroporous microcarriers carrying human mesenchymal stem cells [29]. In each of these studies, the cellularized microcarriers were placed into cylindrical perfusion culture chambers to facilitate cell-based joining of microcarriers into 1–2 cm-sized tissue constructs. Here we utilized vascular cell-containing macroporous gelatin microcarriers (Cultisphers) in conjunction with agarose molds to facilitate 3D tissue engineering of living tubular constructs and evaluated their histological and material properties.

Materials and methods

Cells

Human umbilical vein endothelial cells (HUVECs, Lonza; Basel, Switzerland) were maintained in humidified 5% CO_2, 95% air in Endothelial Growth Medium-2 (EGM-2; Lonza), containing 2% fetal bovine serum. Human aortic smooth muscle cells (HASMCs, Lonza) were maintained in humidified 5% CO_2, 95% air in Smooth Muscle Growth Medium (SMGM; Lonza), containing 5% fetal bovine serum.

Cell culture on microcarriers

Gelatin CultiSpher-G cell carriers (Percell Biolytica, Astorp, Sweden), with an average particle diameter of 130–380 μm and pore size of 20 μm, were purchased from Sigma Chemical Co. (St. Louis, MO). Dry microcarriers were rehydrated, autoclaved and preincubated in cell culture medium according to manufacturer instructions. Microcarriers were then seeded with a 1:1 ratio of HUVECs:HASMCs (each at passage 4–5). Typically, a total of 8×10^6 cells were added to 50 ml of medium (1:1 mixture of EGM-2 and SMGM) containing 0.1 g microcarriers in a 125 ml siliconized Techne biological stirrer flask (R&D Systems, Minneapolis, MN). The cell-microcarrier suspension was subjected to an intermittent stirring regime (30 min at 0 rpm, 2 min at 50 rpm) on a Techne Biological Stirrer (model MCS-104S) for 24 h at 37°C in a humidified 5% CO_2 incubator. The volume of culture medium in the flask was then increased by addition of 50 ml of medium and the stirring speed switched to a continuous 50 rpm. Every 24 h, half of the medium volume was replaced with fresh medium.

Short tube formation in agarose molds

A template for making 4 mm diameter tubular agarose molds in 6 well tissue culture plates (Falcon; Becton Dickinson, Franklin Lakes, NJ) was manufactured from acrylic and PEEK (polyetheretherketone) (Fig. 1A). Agarose molds were made using the template, equilibrated with medium and loaded with microcarriers as follows: Molten 2.0% agarose (Low EEO, J.T. Baker Chemical Co., Phillipsburg, NJ) in Dulbecco's phosphate buffered saline (PBS) was added to wells (3 ml/well) and the template immediately put in place. After the agarose solidified, the template was removed and 2 ml of 1:1 mixture of EGM-2 and SMGM was added and incubated for 24 h at 37°C in a humidified 5% CO_2 incubator. The medium was replaced with fresh medium and placed in the incubator for 2 h. The medium was then removed by aspiration including the residual medium in the tubular molds. Cell-laden microcarriers (grown for 5 days in suspension culture) were drawn up into a 200-μl micropipette tip cut to create a roughly 4 mm bore opening. Microcarriers were allowed to settle in the tip and then dispensed into the molds. Medium (4 ml) was then added to each plate well, covering the filled molds. The plates were incubated at 37°C, 5% CO_2 and the medium replaced every 24 h. Tubular constructs were removed from molds using a pipette tip.

Stacked tube culture

After 5 days in agarose molds, tubular constructs were removed and stacked onto 2 mm diameter stainless steel center post guides mounted on an acrylic base plate in wells of 6-well plates. The stacked tubes were submerged in 1:1 mixture of EGM-2 and SMGM and cultured for varying periods of time.

Histological staining and immunohistochemistry

For histochemical staining, tubular constructs were fixed in 4% paraformaldehyde, PBS pH 7.4, embedded in OCT and subjected to frozen sectioning (10 μm thickness). Frozen sections were subjected to hematoxylin and eosin staining (H&E), Movat's modified pentachrome and Masson's trichrome staining according to standard procedures. Frozen sections of tubular constructs were also subjected to Picrosirius red staining and viewed with polarized light under dark-field optics to detect the birefringence of collagen fibers as described [30]. For immunohistochemical staining, constructs were fixed, embedded in OCT and cryosectioned as above. Sections were then permeabilized in 0.02% Triton-X 100, PBS for 30 min at room temperature (RT) and then incubated with 1.0% BSA, PBS for 1 h at RT. Sections were incubated with primary antibodies i.e., rabbit anti-bovine tropoelastin (provided by Dr. Robert Mecham, Washington University, St. Louis, MO), mouse monoclonal anti-smooth muscle alpha actin (Sigma) or goat anti-VE cadherin (Santa Cruz Biotechnology, Inc., Santa Cruz, CA) diluted in 1.0% BSA, PBS. After an 18 h incubation in a humidified chamber at 4°C, secondary antibodies i.e., Alexa Fluor 488 conjugated donkey anti-goat IgG (Life Technologies, Carlsbad, CA) or Alexa Fluor 568 conjugated donkey anti-rabbit IgG (Life Technologies) were added. Nuclei were stained by incubation of sections with 2.5 μg/ml Hoechst 33258 (Molecular Probes, Life Technologies, Eugene, OR) in PBS for 15 min at RT. TUNEL assays were carried as per the instructions provided with the ApopTag Fluorescein In Situ Apoptosis Detection kit by Chemicon (Temecula, CA). For en face immunohistochemical analysis, tubular constructs were opened by making a slice in the wall, along the longitudinal axis of the tube. The sliced tube was then mounted flat with the lumenal surface facing upward. The orientation of the whole mounted construct was preserved during antibody labeling and confocal imaging.

qPCR analysis

Total RNA was isolated using a Qiagen RNeasy Plus Mini Kit. RNA quality and concentration was determined using an Agilent 2100 Bioanalyzer. cDNA was prepared from total RNA (1.0 μg) using the iScript cDNA synthesis kit (Bio-Rad, Hercules, CA) according to the manufacturer's specifications. cDNA preparations were used undiluted to measure elastin (ELN) and COL1A1 transcript levels, and at a 1:100 dilution for GAPDH and TATA box BP (TBP) reference transcripts. One μl of cDNA was used in 10-μl reactions with the SsoFast EvaGreen Supermix reagent (Bio-Rad) for GAPDH and TBP. A Taqman reaction was performed to measure ELN and COL1A1 mRNA levels using FastStart Universal Probe master mix (Roche) and Roche Universal probe library probes 25 and 67 for ELN and COL1A1, respectively. Oligonucleotide primers were synthesized by Integrated DNA Technologies (Coralville, IA) (Table 1). Thermal cycling was performed using a Bio-Rad CFX96 Real-Time PCR Detection System (Bio-Rad); all reactions were performed in

triplicate. For TaqMan reactions the cycling parameters were 95°C for 10 min (initial melt); 40 cycles of 95°C for 15 sec; 60°C for 60 sec for annealing and extension. . For SscoFast EvaGreen reactions a two-step amplification system with a melt curve was employed. The cycling parameters were 95°C for 2 min (initial melt); 40 cycles of 95°C for 10 sec; 60°C for 30 sec for annealing and extension. The melt curve was from 65°C-95°C, held for 5 sec at each 1°C increment. The resulting data were analyzed with the PCR Miner Web tool [31] to calculate reaction efficiencies and cycle thresholds; the method of Liu and Saint [32] was used to calculate starting fluorescence values (mRNA levels) for genes of interest and reference genes (GAPDH and TBP). Genes of interest were standardized in relation to the reference genes.

Biomechanical testing

A uniaxial ring test was used to probe the passive mechanical response of tube-shaped constructs. To initiate mechanical testing, tubular constructs were removed from agarose molds after 7, 12 and 17 days of culture and immediately secured onto horizontally-oriented 25 gauge cannulas mounted to the upper and lower arms of a uniaxial mechanical tester (Bose Enduratec 3200) (Fig. 5A and B). Samples were kept hydrated with culture medium while being mechanically preconditioned with three tensile displacement cycles up to 1.2 mm (20–25% strain) at a displacement rate of 0.01 mm/s. An identical fourth cycle was then immediately performed, during which load data (50 points/s) was recorded by system software (Wintest). An image-based technique was used to measure the local strain in the middle section of each sample. Immediately following sample mounting, blue tissue marking dye was applied by a fine tip applicator to create a dot pattern. A series of images was captured throughout testing using a Nikon SMZ-U light microscope and a Q-Imaging camera. Using ImagePro 5.1 to spatially calibrate the image, the vertical distances between the dots were calculated to facilitate measurement of local strain. Similar testing was performed on samples that had been decellularized using a hypotonic treatment with deionized water followed by a treatment with sodium dodecyl sulfate (SDS) in Dulbecco's PBS as previously described [33].

Results

Cellularized Cultisphers fuse to form tubular structures

Using a custom template (Fig. 1A), tubular agarose molds were made in 6 well tissue culture plates (Fig. 1B). After equilibration of the agarose molds with culture medium, cellularized Cultisphers were dispensed into the molds and cultured for varying periods. After 3–5 days in culture, the cellularized beads had joined together such that intact tubular structures (~4 mm diameter × ~2.5 mm long having a ~2 mm bore) could easily be removed from the molds (Fig. 1C and D). Low magnification microscopic examination of the tubular constructs revealed closely packed microcarrier beads and inter-bead material including evidence of material lining the lumenal and ablumenal surfaces of the tubes (Fig. 1E and F).

Analysis of H&E stained sections from the tubular constructs (cultured 7 days in agarose molds) showed that the areas located between Cultisphers were rich with cells (Fig. 2A and B, *arrowheads*). Perhaps most remarkable was the presence of layers of cells lining the

lumenal and ablumenal surfaces of the nascent tubes, forming an epithelium-like morphology (Fig. 2A and B, *arrows*). Immunohistological analysis of frozen sections of the tubular constructs was performed using antibodies to the smooth muscle cell marker, SM alpha actin, and the endothelial cell marker, VE-cadherin (Fig. 2C and D). SM alpha actin-expressing cells were associated with the Cultisphers and the regions between Cultisphers. The lumenal and ablumenal epithelium-like cell layers contained both VE-cadherin expressing cells and SM alpha actin expressing cells. The cell layer lining the lumens of the tubes appeared to be comprised of VE-cadherin expressing cells overlying SM alpha actin expressing cells (Fig. 2D).

Stacked tubes fuse to form elongated tubes

Tubes made from the cellularized Cultisphers were also evaluated for their capacity to join with other tubes. After 5 days in agarose molds, the short tubes (~2.5 mm long) were removed and stacked onto 2 mm diameter center post guides immersed in medium for 3–10 days. Within the stacked configuration, juxtaposed tubes fused via inter-tube cellular bridges (Fig. 3A–D). Using this approach elongated tubular structures comprised of 2, 3 and 4 tubes were easily formed. Inspection of the inter-tube joints revealed cellular bridges.

Elastin and collagen in Cultispher tubular constructs

Sections of Cultispher tube constructs cultured for 7–17 days in agarose molds were subjected to histochemical analysis. Using Masson's trichrome staining, which stains collagen fibers blue; little blue stain was detectable in the tubular constructs cultured 7 days in agarose molds (Fig. 4A and B). By contrast, pronounced blue Masson's trichrome staining was present in inter-microcarrier bead regions of constructs cultured for 12 and 17 days in agarose molds (Fig. 4C–F).

Sections of the Cultispher tube constructs cultured for 7–17 days in agarose molds were also subjected to Picrosirius red staining and examined by polarized light microscopy. In 7-day constructs, the regions located between microcarrier beads were found to contain numerous fiber-like structures that show green/yellow birefringence (Fig. 4G and H, *arrows*), characteristic of newly deposited or less cross-linked collagen. Fibers having green/yellow birefringence could be found that were aligned circumferential to the lumen. Green/yellow fibers were also widely distributed throughout the day 12 and 17 constructs with relatively higher levels of green/yellow birefringence apparent in association with the epithelial layers (Fig. 4I–L). Over time, the relative levels of red/orange birefringence, which is characteristic of mature cross-linked collagen, appeared to increase in association with the layers of cells lining the lumenal and ablumenal surfaces of the tubes (Fig. 4L). We also observed that over time the relative level of red/orange birefringence associated construct-embedded Cultisphers diminished, concomitant with the progressive reduction in Cultispher size, perhaps reflective of a degradative process.

Immunohistological staining was performed to evaluate elastin deposition in the 7, 12 and 17-day constructs. Analysis of the constructs in cross section showed punctate deposits of elastin immunolabel, in interbead regions and regions associated with the epithelial-like layers (Fig. 4M–R). With time in culture, the relative intensity of anti-elastin

immunolabeling appeared to increase. Confocal analysis of anti-elastin stained whole mounts, cut to permit en face examination of the luminal surface, revealed fibrillar configurations, with elastin-containing fibers often oriented parallel to one another (Fig. 4S and T). Since control reactions showed that cell-free Cultispheres were weakly positive for anti-elastin (i.e., diffuse staining, never fibrillar) (Fig. 4U), it is possible that the Cultispher manufacturing procedure might allow for dermal elastin to be a component in addition to porcine skin gelatin. For this reason, our interpretations of the immunohistological analysis of elastin were focused on extra-Cultispher regions of the constructs i.e., inter-Cultispher bead regions and the layers of cells lining the lumenal and ablumenal surfaces of the tubes. As evidence for the specificity of the anti-elastin immunolabeling, controls showed no reactivity by the fluorochrome conjugated secondary antibody in the absence of primary antibody, as well as positive detection of elastin in the ascending aorta (Fig. 4X).

qPCR analysis was performed to quantify levels of collagen (COL1A1) and tropoelastin (ELN) mRNA expressed by cells in the tubular constructs during the 7–12 day culture period as compared to ECs and VSMCs cultured in 2D. The levels of COL1A1 and ELN expressed by microcarriers containing co-cultures of ECs and VSMCs were higher than levels expressed by the cells cultured individually in 2D culture. Moreover, both COL1A1 and ELN mRNA levels were found to increase, then decrease during the period when the cellularized microcarriers were cultured in the molds, with peak levels at 12 days of culture (Fig. 5). The decrease in COL1A1 and ELN mRNA levels in 17-day constructs could be related to an increased level of apoptosis. TUNEL analysis showed an increase in apoptosis between 7- and 17-day constructs (15 ± 6.1% TUNEL positive nuclei for 7 day constructs; 37 ± 17.6% TUNEL positive nuclei for 17 day constructs; p=0.0498; based on analysis of nuclei in multiple optical fields in sections from several 7 and 17 day constructs using Fisher's Exact Test, 2 tails).

Tubular constructs exhibit progressive stiffening with prolonged culture periods

Mechanical testing was performed on tubular constructs that had been cultured for 7, 12, or 17 days in agarose molds. The uniaxial mechanical response of all examined Cultispher tubes (outer diameter= 3.93 ± 0.41 mm, wall thickness= 1.16 ± 0.24 mm and wall height= 2.10 ± 0.35 mm; n = 20) was retained over multiple loading cycles, indicating that the materials behave as elastic solids. There was little evidence of damage accumulation, which would be reflected by a progressive decrease in the peak load at later cycles. Load and local displacement data were processed to yield Cauchy stress σ and stretch ratio λ as follows,

$$\sigma = \frac{F}{A} and \lambda = \frac{L}{L_0} \quad \text{Eq. 1}$$

where F is the measured load, A is the current cross-sectional area, L is the current test segment length, and L_0 is the initial test segment length. All materials exhibited a high degree of nonlinearity in the examined range, with a notable shifting of curves with prolonged culture time (Fig. 6C). The observed mechanical behavior of the constructs is qualitatively similar to that of native vascular tissue, where it is well-accepted that the low strain mechanical response is governed by elastin, while the high-strain response reflects the mechanical contribution of collagen [34]. Linearization of the data over low stretch ratios (1 <

$\lambda < 1.08$) was used to calculate an elastic modulus that reflects the elastin-dominated portion of the mechanical response, denoted here as $E_{elastin}$. Increased culture time led to a monotonic increase in $E_{elastin}$, which ranged from 9.9± 6.2 kPa at 7 days (n=5) to 104.5 ± 60.4 kPa at 17 days (n=5). Similarly, an elastic modulus referring to linearized data over higher stretch ratios ($1.1 < \lambda < 1.2$) was calculated to quantify the collagen-mediated portion of the mechanical response, $E_{collagen}$, and also dramatically increased from 78.9 ± 23.4 kPa at 7 days (n=5) to 1278.1 ± 329.3 kPa at 17 days (n=5). A two-way ANOVA with critical p-value = 0.05 and a post-hoc Tukey test with $\alpha = 0.05$ indicate there was a statistically significant increase in both $E_{elastin}$ and $E_{collagen}$ between 7 and 17 day constructs.

Decellularized tubular constructs exhibit mechanical behavior similar to that of living constructs

Living constructs were treated with hypotonic and hypertonic rinses and SDS to obtain acellular ring constructs. The uniaxial mechanical response of decellularized 17 day constructs (inset panel of Fig. 6D)was nearly identical to that of living constructs cultured for the same amount of time (Fig. 6D). Two-way ANOVA analyses revealed that while culture time is a statistically significant factor in determining $E_{elastin}$ and $E_{collagen}$, cellularization state and the interaction between the two are insignificant factors. Moreover, a post-hoc Tukey test with $\alpha = 0.05$ indicates statistically insignificant differences in both moduli of the cellularized and decellularized 17 day samples.

Discussion

Here we demonstrate that cellularized gelatin macroporous microcarriers (i.e., Cultisphers) can be used as self-adhering building blocks for the fabrication of tubular structures. The ability of cellularized Cultisphers to adhere to one another involved the formation of both cellular and ECM bridging between microcarrier beads. Cellular bridges included cells occupying the inter-bead spaces as well as epithelium-like cell layers lining the lumenal and ablumenal surfaces of the tubular constructs. The propensity of cellularized Cultisphers to form cellular bridges was apparent even when they were in suspension culture, as evidenced by the formation of aggregates interconnected by both VE-cadherin-positive and SM alpha actin-positive cells. While the present studies employed Cultisphers laden with endothelial cells and vascular smooth muscle cells, we also found that Cultisphers containing co-cultures of endothelial cells and the multipotent mouse cell line, C3H10T1/2, underwent inter-microcarrier bead cellular bridging (*data not shown*). By contrast, little to no inter-microcarrier bead cellular bridging was apparent when Cultisphers containing only endothelial cells (HUVECs) were used (*data not shown*). This observation is similar to other findings showing that co-culture of endothelial cells with retinal cells on microcarrier beads was required to stimulate endothelial cells to form endothelial cords that interconnect microcarrier beads [35].

A potential application of the cellularized microcarrier-based fabrication approach described here is in the manufacture of replacement tubular tissue structures damaged by injury or disease. For example, each year hundreds of thousands of people undergo vein or artery replacement therapy [36]; however, systemic vascular disease often means that autologous

replacement blood vessels are not available. Cellularized microcarrier-based fabrication is a cell-based approach to blood vessel construction that might permit synthesis of living prostheses having cellular composition and mechanical properties comparable to the walls of native blood vessels. The clinical applicability of microcarrier-based fabrication of living tubular constructs will require that the cellular components be derived from a patient's own tissues. One source for autologous cells is adipose tissue. Indeed, vascular cells have been isolated from the vascular fraction of human adipose tissue [37, 38] and human adipose-derived stem cells have been used to produce endothelial cells and smooth muscle cells [39–41].

In addition to fabrication and biomechanical testing of living microcarrier-based constructs, we also demonstrated that acellular ECM scaffolds could be generated from the living constructs using a standard decellularization protocol [33]. Biomechanical testing of acellular ECM scaffolds showed that decellularization did not significantly alter the mechanical behavior of constructs, implying that ECM mediators of the mechanical response are not compromised by the decellularization process. The retention of mechanical properties increases the potential of these scaffolds to serve as clinical biomaterials (e.g., off the-shelf tissue-engineered vascular scaffolds).

Engineered tissues need to display strength and compliance necessary to sustain mechanical integrity in response to physiological mechanical forces. In tissues such as arterial blood vessels collagens and elastin provide these properties [42–44]. Analysis of the ECM composition of the tubes generated from Cultispher microcarriers containing vascular cells revealed the presence of collagen in inter-microcarrier bead regions and associated with the lumenal and ablumenal epithelium-like layers. Importantly, relative levels of collagen deposition in the tubes appeared to increase with duration of time in culture, which is consistent with the progressive stiffening measured by mechanical testing of 7, 12 and 17-day tubes. Elastin expression in the constructs was also demonstrated immunologically and using qPCR. Quantitative and qualitative deficiencies in the process of elastogenesis are impediments to the engineering of tissues such as blood vessels requiring functional elastin architecture [45]. En face analysis of the anti-elastin labeled tubular constructs revealed extensive deposition of elastin into elongated fibers, often observed oriented in parallel configurations.

Biomechanical testing of the tubes generated from cellularized Cultisphers displayed mechanical behavior consistent with that of an isotropic, incompressible, homogeneous, elastic material. A modulus of 104.5 ± 60.4 kPa ($E_{elastin}$) was calculated from the elastin-dominated portion of the mechanical response of 17-day constructs and a modulus of 1278.1 ± 329.3 kPa was calculated from the collagen-dominated portion of the mechanical response. By comparison, incremental Young's moduli of the intact wall (both the tunica adventitia and tunica media layers) of human carotid arteries have been reported to be equal to 160 ± 40 kPa and 900 ± 250 kPa for the low strain region and the high strain region, respectively [46]. Isolated insoluble elastin and elastin-rich tissues (e.g., bovine nuchal ligament) have been shown to behave as a nearly linear elastic material with Young's modulus of roughly 400–800 kPa, depending on the tissue source and isolation procedures [34, 46–48]. Biomaterials produced by cross-linking recombinant elastin polypeptides show similar behavior with a lower modulus of about 250 kPa [49]. More recent

studies [50] suggest that aortic elastin shows some anisotropy in its material behavior, with axial stiffness being less than circumferential stiffness. The $E_{elastin}$ modulus of the Cultispher tube constructs is consistent with the lower end of the range reported by Zou and Zhang [50] for the axial tangent modulus of isolated aortic elastin at low strains.

The relatively low $E_{elastin}$ of the Cultispher tube constructs may be an indication that the elastin produced in the constructs in not highly cross-linked. Previous work by the Wang group demonstrated production of mature elastin in baboon VSMC-seeded tubular scaffolds fabricated from porous poly(glycerol sebacate) and cultured in a pulsatile flow bioreactor for 3 weeks [51]. Interestingly, these authors reported a significant effect of scaffold pore size on elastin production and mechanical properties; with constructs having the smallest pores (25–32 m) attaining the highest values of both elastic modulus (~60 kPa) and ultimate tensile strength [51]. In the current work, we achieved comparable elastic modulus values after 17 days in static culture, without any mechanical pre-conditioning. The macroporous gelatin microcarriers used in our study have a pore size at the low end of the range examined by Lee, et. al, [51]. Therefore, we might expect that mechanical pre-conditioning of Cultispher-based constructs (e.g., application of cyclical strain or flow) would lead to further improvement in their mechanical properties.

Acknowledgments

This work was supported by the National Science Foundation/EPSCoR Grant (EPS-0903795) and by NSF CMMI-1200358. We thank Dr. Amy Bradshaw for providing expert advice on Picrosirius red staining and polarized light microscopy. We thank Michael Gore (University of South Carolina School of Medicine) for his fabrication of templates.

References

1. Desai M, Seifalian AM, Hamilton G. Role of prosthetic conduits in coronary artery bypass grafting. Eur. J. Cardiothorac. Surg. 2011; 40(2):394–398. [PubMed: 21216613]
2. L'Heureux N, Paquet S, Labbe R, Germain L, Auger FA. A completely biological tissue-engineered human blood vessel. FASEB J. 1998; 12(1):47–56. [PubMed: 9438410]
3. Mitchell SL, Niklason LE. Requirements for growing tissue-engineered vascular grafts. Cardiovasc Pathol. 2003; 12(2):59–64. [PubMed: 12684159]
4. Borschel GH, Huang YC, Calve S, Arruda EM, Lynch JB, Dow DE, Kuzon WM, Dennis RG, Brown DL. Tissue engineering of recellularized small-diameter vascular grafts. Tissue Eng. 2005; 11(5–6):778–786. [PubMed: 15998218]
5. Kielty CM, Stephan S, Sherratt MJ, Williamson M, Shuttleworth CA. Applying elastic fibre biology in vascular tissue engineering. Philos. Trans. R. Soc. Lond. B. Biol. Sci. 2007; 362(1484):1293–1312. [PubMed: 17588872]
6. Wang X, Lin P, Yao Q, Chen C. Development of small-diameter vascular grafts. World J. Surg. 2007; 31(4):682–689. [PubMed: 17345123]
7. Naito Y, Shinoka T, Duncan D, Hibino N, Solomon D, Cleary M, Rathore A, Fein C, Church S, Breuer C. Vascular tissue engineering: towards the next generation vascular grafts. Advanced drug delivery reviews. 2011; 63(4–5):312–323. [PubMed: 21421015]
8. Swartz DD, Russell JA, Andreadis ST. Engineering of fibrin-based functional and implantable small-diameter blood vessels. American journal of physiology. Heart and circulatory physiology. 2005; 288(3):H1451–H1460. [PubMed: 15486037]
9. Hibino N, McGillicuddy E, Matsumura G, Ichihara Y, Naito Y, Breuer C, Shinoka T. Late-term results of tissue-engineered vascular grafts in humans. J. Thorac. Cardiovasc. Surg. 2010; 139(2): 431–436. 436 e431–432. [PubMed: 20106404]

10. Buttafoco L, Engbers-Buijtenhuijs P, Poot AA, Dijkstra PJ, Vermes I, Feijen J. Physical characterization of vascular grafts cultured in a bioreactor. Biomaterials. 2006; 27(11):2380–2389. [PubMed: 16289328]
11. van Wezel AL. Growth of cell-strains and primary cells on micro-carriers in homogeneous culture. Nature. 1967; 216(5110):64–65. [PubMed: 4292963]
12. Hirtenstein M, Clark J, Lindgren G, Vretblad P. Microcarriers for animal cell culture: a brief review of theory and practice. Dev. Biol. Stand. 1980; 46:109–116. [PubMed: 6153997]
13. Clark JM, Hirtenstein MD. Optimizing culture conditions for the production of animal cells in microcarrier culture. Ann. N. Y. Acad. Sci. 1981; 369:33–46. [PubMed: 6942784]
14. Mignot G, Faure T, Ganne V, Arbeille B, Pavirani A, Romet-Lemonne JL. Production of recombinant Von Willebrand factor by CHO cells cultured in macroporous microcarriers. Cytotechnology. 1990; 4(2):163–171. [PubMed: 1370026]
15. Nikolai TJ, Hu WS. Cultivation of mammalian cells on macroporous microcarriers. Enzyme Microb. Technol. 1992; 14(3):203–208. [PubMed: 1372509]
16. Malda J, Frondoza CG. Microcarriers in the engineering of cartilage and bone. Trends Biotechnol. 2006; 24(7):299–304. [PubMed: 16678291]
17. Martin Y, Eldardiri M, Lawrence-Watt DJ, Sharpe JR. Microcarriers and their potential in tissue regeneration. Tissue engineering Part B Reviews. 2011; 17(1):71–80. [PubMed: 21083436]
18. Voigt M, Schauer M, Schaefer DJ, Andree C, Horch R, Stark GB. Cultured epidermal keratinocytes on a microspherical transport system are feasible to reconstitute the epidermis in full-thickness wounds. Tissue Eng. 1999; 5(6):563–572. [PubMed: 10611548]
19. Liu JY, Hafner J, Dragieva G, Seifert B, Burg G. Autologous cultured keratinocytes on porcine gelatin microbeads effectively heal chronic venous leg ulcers. Wound Repair Regen. 2004; 12(2): 148–156. [PubMed: 15086765]
20. Kim SS, Gwak SJ, Choi CY, Kim BS. Skin regeneration using keratinocytes and dermal fibroblasts cultured on biodegradable microspherical polymer scaffolds. Journal of biomedical materials research Part B, Applied biomaterials. 2005; 75(2):369–377.
21. Gustafson CJ, Birgisson A, Junker J, Huss F, Salemark L, Johnson H, Kratz G. Employing human keratinocytes cultured on macroporous gelatin spheres to treat full thickness-wounds: an in vivo study on athymic rats. Burns. 2007; 33(6):726–735. [PubMed: 17467913]
22. Eldardiri M, Martin Y, Roxburgh J, Lawrence-Watt DJ, Sharpe JR. Wound contraction is significantly reduced by the use of microcarriers to deliver keratinocytes and fibroblasts in an in vivo pig model of wound repair and regeneration. Tissue engineering. Part A. 2012; 18(5–6):587–597. [PubMed: 21939396]
23. Lippens E, Vertenten G, Girones J, Declercq H, Saunders J, Luyten J, Duchateau L, Schacht E, Vlaminck L, Gasthuys F, Cornelissen M. Evaluation of bone regeneration with an injectable, in situ polymerizable Pluronic F127 hydrogel derivative combined with autologous mesenchymal stem cells in a goat tibia defect model. Tissue engineering. Part A. 2010; 16(2):617–627. [PubMed: 19743958]
24. Yang Y, Hallgrimsson B, Putnins EE. Craniofacial defect regeneration using engineered bone marrow mesenchymal stromal cells. Journal of biomedical materials research. Part A. 2011; 99(1): 74–85. [PubMed: 21800417]
25. Clavijo-Alvarez JA, Nguyen VT, Santiago LY, Doctor JS, Lee WP, Marra KG. Comparison of biodegradable conduits within aged rat sciatic nerve defects. Plast. Reconstr. Surg. 2007; 119(6): 1839–1851. [PubMed: 17440364]
26. Seland H, Gustafson CJ, Johnson H, Junker JP, Kratz G. Transplantation of acellular dermis and keratinocytes cultured on porous biodegradable microcarriers into full-thickness skin injuries on athymic rats. Burns. 2011; 37(1):99–108. [PubMed: 20630659]
27. Palmiero C, Imparato G, Urciuolo F, Netti P. Engineered dermal equivalent tissue in vitro by assembly of microtissue precursors. Acta biomaterialia. 2010; 6(7):2548–2553. [PubMed: 20102750]
28. Mei Y, Luo H, Tang Q, Ye Z, Zhou Y, Tan WS. Modulating and modeling aggregation of cell-seeded microcarriers in stirred culture system for macrotissue engineering. J. Biotechnol. 2010; 150(3):438–446. [PubMed: 20888876]

29. Chen M, Wang X, Ye Z, Zhang Y, Zhou Y, Tan WS. A modular approach to the engineering of a centimeter-sized bone tissue construct with human amniotic mesenchymal stem cells-laden microcarriers. Biomaterials. 2011; 32(30):7532–7542. [PubMed: 21774980]
30. Bradshaw AD, Baicu CF, Rentz TJ, Van Laer AO, Bonnema DD, Zile MR. Age-dependent Alterations in Fibrillar Collagen Content and Myocardial Diastolic Function: Role of SPARC in Post-Synthetic Procollagen Processing. American journal of physiology. Heart and circulatory physiology. 2009; 298:H614–H622. [PubMed: 20008277]
31. Zhao S, Fernald RD. Comprehensive algorithm for quantitative real-time polymerase chain reaction. J. Comput. Biol. 2005; 12(8):1047–1064. [PubMed: 16241897]
32. Liu W, Saint DA. Validation of a quantitative method for real time PCR kinetics. Biochem. Biophys. Res. Commun. 2002; 294(2):347–353. [PubMed: 12051718]
33. Seif-Naraghi SB, Horn D, Schup-Magoffin PA, Madani MM, Christman KL. Patient-to-patient variability in autologous pericardial matrix scaffolds for cardiac repair. Journal of cardiovascular translational research. 2011; 4(5):545–556. [PubMed: 21695575]
34. Roach MR, Burton AC. The reason for the shape of the distensibility curves of arteries. Canadian journal of biochemistry and physiology. 1957; 35(8):681–690. [PubMed: 13460788]
35. Dutt K, Sanford G, Harris-Hooker S, Brako L, Kumar R, Sroufe A, Melhado C. Three-dimensional model of angiogenesis: coculture of human retinal cells with bovine aortic endothelial cells in the NASA bioreactor. Tissue Eng. 2003; 9(5):893–908. [PubMed: 14633374]
36. Epstein AJ, Polsky D, Yang F, Yang L, Groeneveld PW. Coronary revascularization trends in the United States, 2001–2008. JAMA. 2011; 305(17):1769–1776. [PubMed: 21540420]
37. Kern PA, Knedler A, Eckel RH. Isolation and culture of microvascular endothelium from human adipose tissue. J. Clin. Invest. 1983; 71(6):1822–1829. [PubMed: 6306056]
38. Lin K, Matsubara Y, Masuda Y, Togashi K, Ohno T, Tamura T, Toyoshima Y, Sugimachi K, Toyoda M, Marc H, Douglas A. Characterization of adipose tissue-derived cells isolated with the Celution system. Cytotherapy. 2008; 10(4):417–426. [PubMed: 18574774]
39. Zuk PA, Zhu M, Mizuno H, Huang J, Futrell JW, Katz AJ, Benhaim P, Lorenz HP, Hedrick MH. Multilineage cells from human adipose tissue: implications for cell-based therapies. Tissue Eng. 2001; 7(2):211–228. [PubMed: 11304456]
40. Rodriguez LV, Alfonso Z, Zhang R, Leung J, Wu B, Ignarro LJ. Clonogenic multipotent stem cells in human adipose tissue differentiate into functional smooth muscle cells. Proc. Natl. Acad. Sci. U. S. A. 2006; 103(32):12167–12172. [PubMed: 16880387]
41. Auxenfans C, Lequeux C, Perrusel E, Mojallal A, Kinikoglu B, Damour O. Adipose-derived stem cells (ASCs) as a source of endothelial cells in the reconstruction of endothelialized skin equivalents. Journal of tissue engineering and regenerative medicine. 2012; 6(7):512–518. [PubMed: 21755603]
42. Mecham, RP.; Davis, EC. Elastic fiber structure and assembly. In: Yurchenco, PD.; Birk, DE.; Mecham, RP., editors. Extracellular matrix assembly and structure. New York, NY: Academic Press; 1994. p. 281-314.
43. Faury G. Function-structure relationship of elastic arteries in evolution: from microfibrils to elastin and elastic fibres. Pathol. Biol. (Paris). 2001; 49(4):310–325. [PubMed: 11428167]
44. Kielty CM, Sherratt MJ, Shuttleworth CA. Elastic fibres. J. Cell Sci. 2002; 115(Pt 14):2817–2828. [PubMed: 12082143]
45. Bashur CA, Venkataraman L. Ramamurthi A. Tissue engineering and regenerative strategies to replicate biocomplexity of vascular elastic matrix assembly. Tissue engineering Part B, Reviews. 2012; 18(3):203–217. [PubMed: 22224468]
46. Hoeve CA, Flory PJ. The elastic properties of elastin. Biopolymers. 1974; 13(4):677–686. [PubMed: 4847581]
47. Lillie MA, Chalmers GW, Gosline JM. The effects of heating on the mechanical properties of arterial elastin. Connect. Tissue Res. 1994; 31(1):23–35. [PubMed: 15609619]
48. Lillie MA, David GJ, Gosline JM. Mechanical role of elastin-associated microfibrils in pig aortic elastic tissue. Connect. Tissue Res. 1998; 37(1–2):121–141. [PubMed: 9643652]

49. Bellingham CM, Lillie MA, Gosline JM, Wright GM, Starcher BC, Bailey AJ, Woodhouse KA, Keeley FW. Recombinant human elastin polypeptides self-assemble into biomaterials with elastin-like properties. Biopolymers. 2003; 70(4):445–455. [PubMed: 14648756]

50. Zou Y, Zhang Y. An experimental and theoretical study on the anisotropy of elastin network. Ann. Biomed. Eng. 2009; 37(8):1572–1583. [PubMed: 19484387]

51. Lee KW, Stolz DB, Wang Y. Substantial expression of mature elastin in arterial constructs. Proc. Natl. Acad. Sci. U. S. A. 2011; 108(7):2705–2710. [PubMed: 21282618]

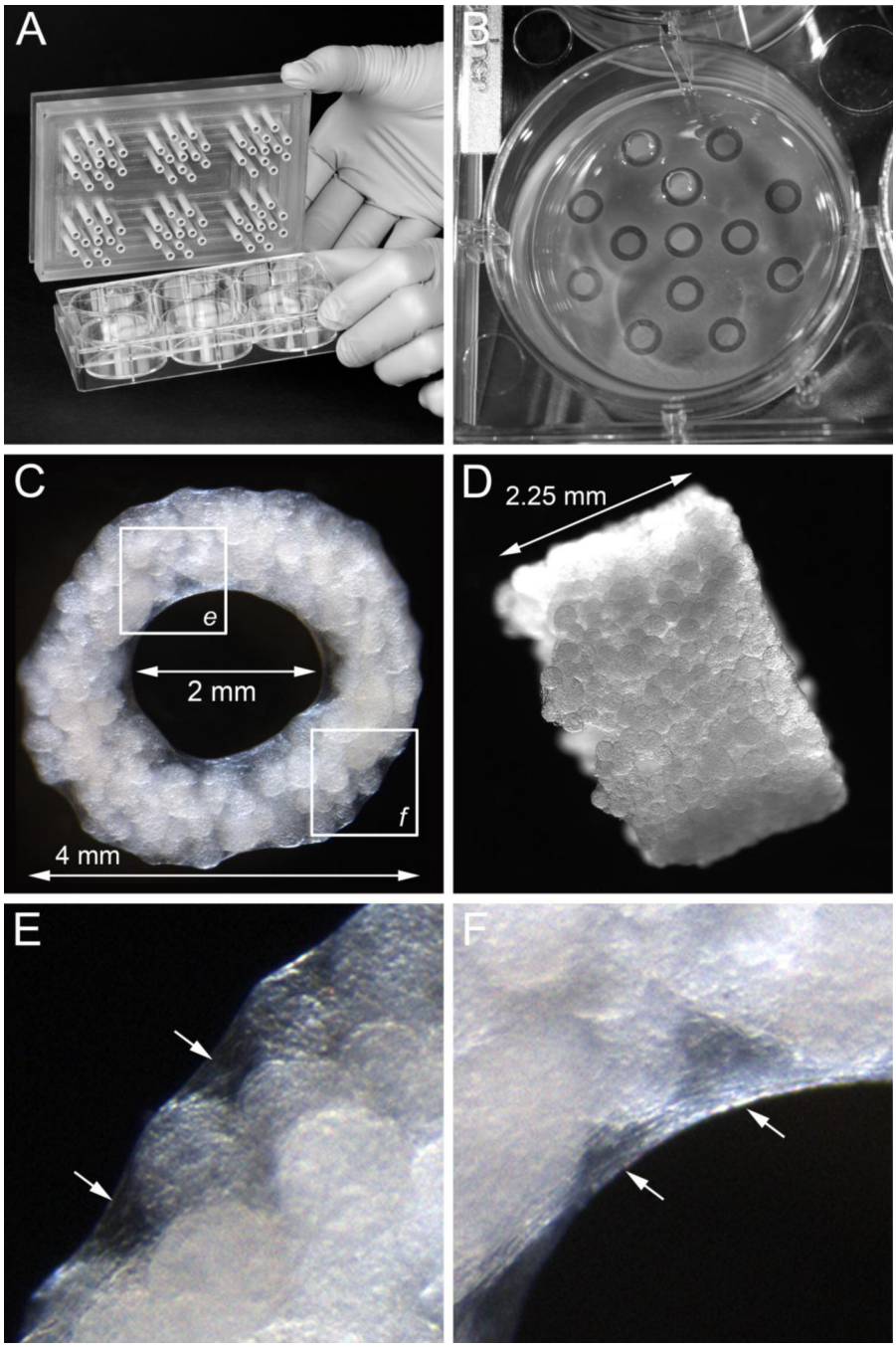

Figure 1.

Cellularized Cultispheres placed in agarose tubular molds assemble to form tubes, *A*, PEEK (polyetheretherketone) template used for generating tubular molds in 6-well culture plates, *B*, tubular agarose molds formed in a well of a 6-well culture plate, *C* and *D, en face* and side views of a tubular construct having an outer diameter of 4 mm, wall thickness of 1 mm, and a height of 2.25 mm, *E* and *F*, high magnification views of the boxed areas in panel *C* showing the inter-microcarrier bead material on the *ablumenal* (*E*) and lumenal (F) surfaces of the tubes (*arrows*).

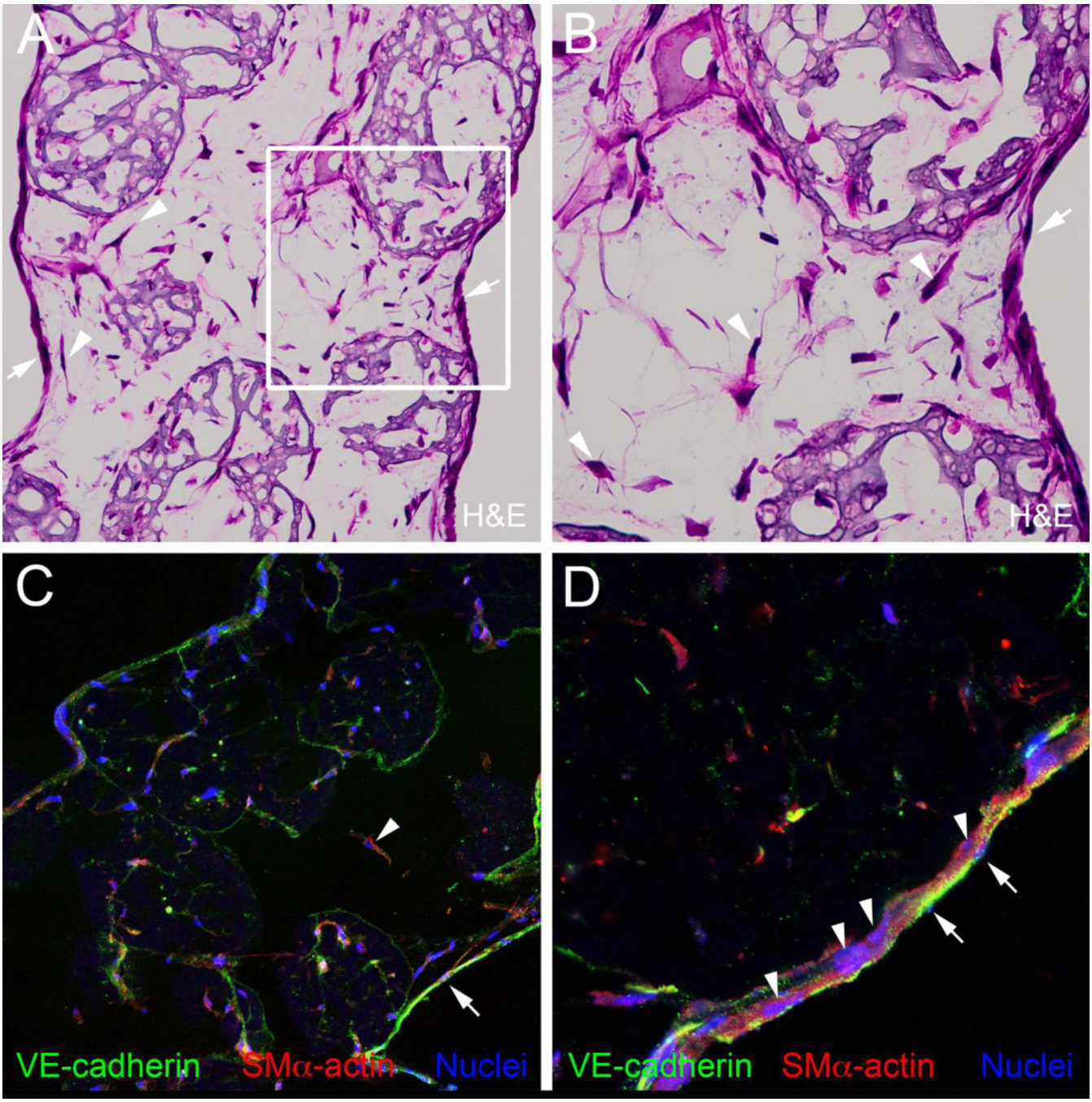

Figure 2.

Tubular constructs have cellularized inter-microcarrier bead regions and lumenal and ablumenal epithelium-like cell layers, *A* and *B*, H&E staining of a frozen section from a tubular construct after 7 days in culture, *Arrows* in A and B point to epithelium-like layers, *Arrowheads* in A and B point to cells located in spaces between Cultispheres, *C* and *D*, anti-VE-cadherin (*green*) and anti-SMα actin (*red*) double immunostaining of a frozen section from a 7-day tubular construct, *Arrows* in C and D point to VE-cadherin-positive cells in the epithelium-like layer lining the lumen of the construct, *Arrowheads* in C and D point to *SMα*

actin-positive cells located in spaces between Cultisphers (C) and subjacent to the lumenal epithelium-like layer (D). In A-D, the ablumenal surface of the tubular construct is on the left and the lumenal surface is on the right.

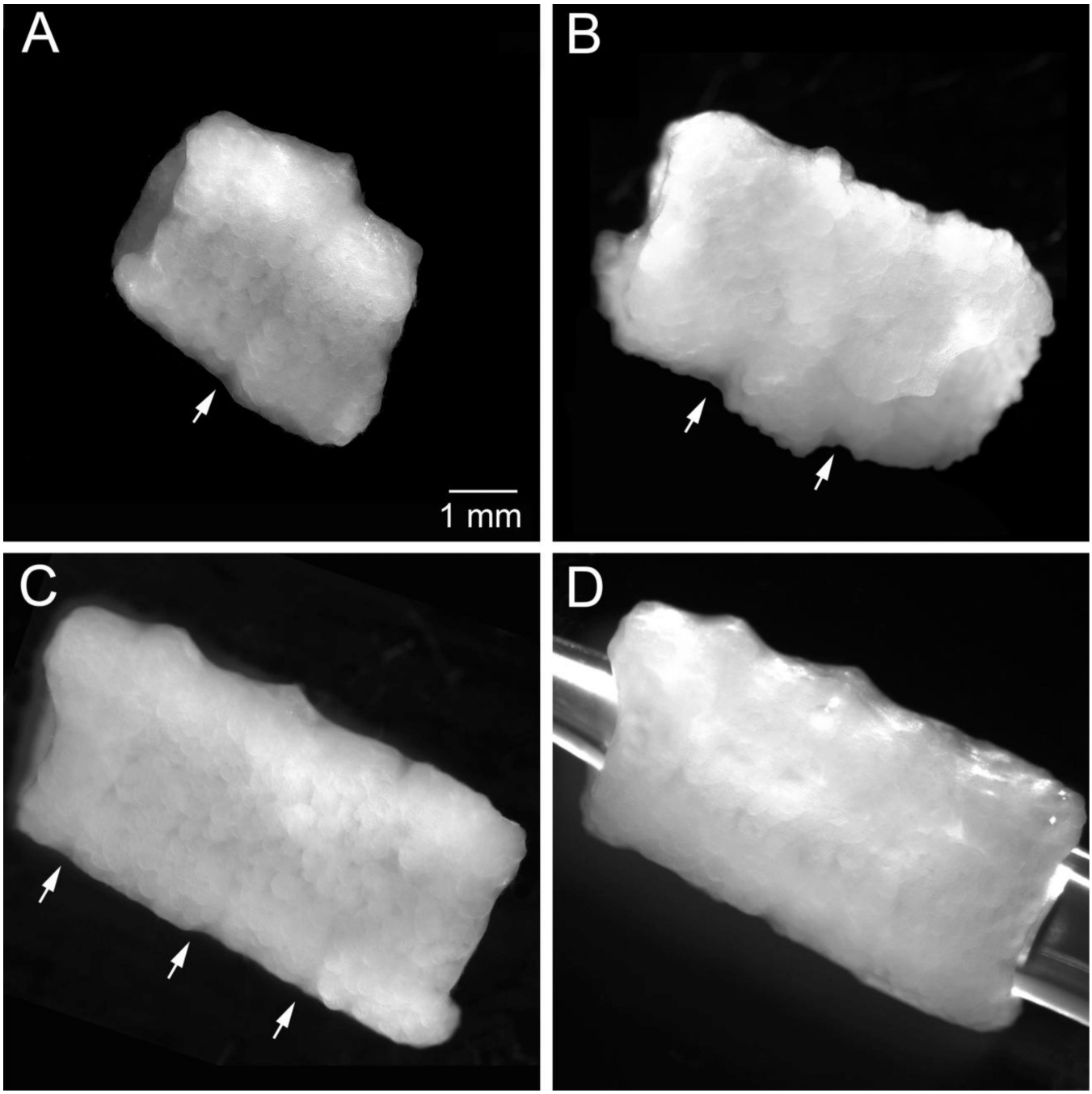

Figure 3.

Stacked tubular constructs join to form elongated tubes, *A*, tubular construct generated by stacking 2 tubular constructs (each ~4 mm diameter × 2.5 mm in height with a 2 mm bore; obtained after 7 days in agarose molds) and culturing for 10 days, *B*, tubular construct generated by stacking 3 tubular constructs and culturing for 3 days, *C*, tubular construct generated by stacking 4 tubular constructs and culturing for 8 days, *D*, tubular construct shown in *C* with a pipette tip inserted to demonstrate a continuous lumen, *Arrows* indicate fused inter-tube joints.

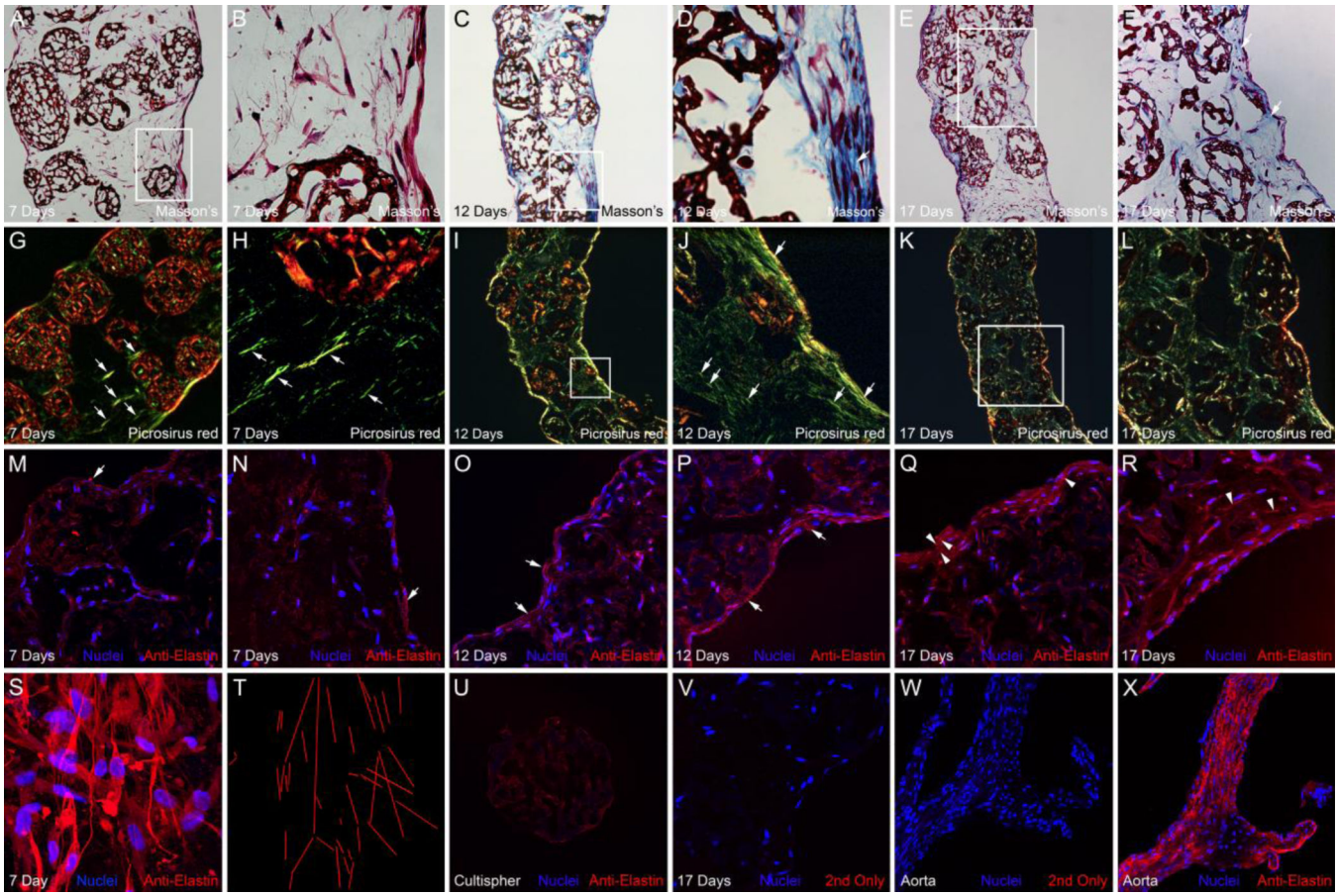

Figure 4.

Histochemical and immunological analysis of collagen and elastin in tubular constructs, *A-F*, show Masson's trichrome staining of frozen sections from tubular constructs cultured for 7, 12 and 17 days, *B*, *D* and *F* are high magnification views of the boxed areas in *A*, *C* and *E*. *Arrows* in *D* and *F* point to areas with pronounced collagen staining associated with lumenal cell layers, *G-L* show cross-polarized light images of Picrosirius red stained frozen sections from tubular constructs cultured for 7, 12 and 17 days, *J* and *L* are high magnification views of the boxed areas in *I* and *K*. *Arrows* point to aligned fibrils, which based on their green/yellow Picrosirius red staining in polarized light are immature collagen fibers, *M-R*, show anti-elastin immunostaining (*red*) of frozen sections from tubular constructs cultured for 7, 12 and 17 days. Nuclei (*blue*) were stained with Hoechst stain. In *A-R* the ablumenal surfaces of the constructs are to the left and the lumenal surfaces are to the right, *Arrows* indicate anti-elastin immunolabeling (*red*) associated with the epithelial layers lining the lumenal and ablumenal surfaces of the construct, *Arrowheads* indicate anti-elastin immunolabeling in continuous configurations, *S* shows an image of an anti-elastin stained whole mount of a tubular construct cultured for 7 days, cut to permit en face examination of the luminal surface, *T*, depicts the parallel orientation of anti-elastin-labeled fibrils shown in panel S, *U* shows a non-cellularized Cultispher microcarrier bead immunolabeled with anti-elastin (*red*), *V* shows a frozen section from a tubular construct cultured for 17 days that was labeled with conjugated secondary antibody (no-primary

antibody) as a negative control, *W* shows conjugated secondary antibody labeling (red) and X shows anti-elastin immunostaining (*red*) of frozen sections from a mouse ascending aorta (adjacent to the aortic root and containing a valve cusp) as a positive control.

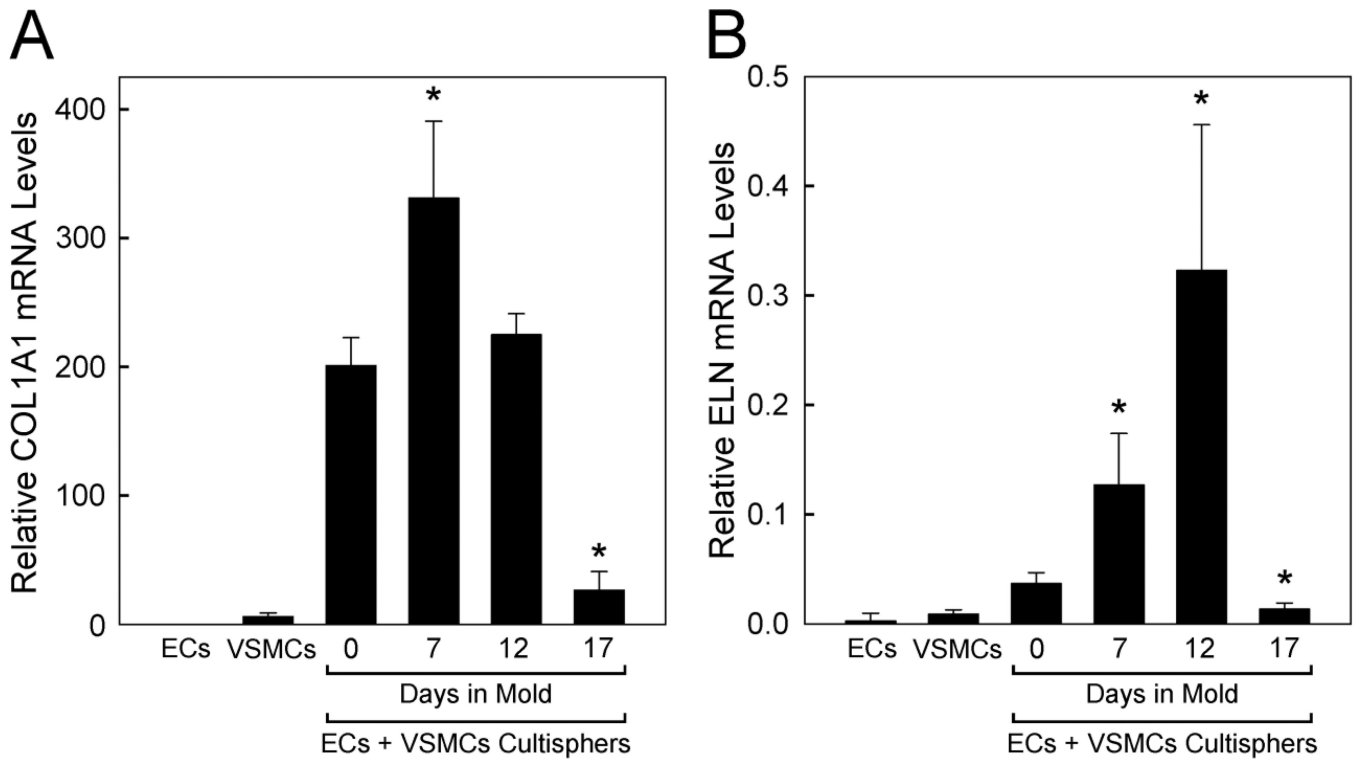

Figure 5.

qPCR analysis of collagen (COL1A1) and elastin (ELN) mRNA expression in vascular cells in 2D culture, vascular cell-containing Cultisphers and tubular constructs. COL1A1 (*A*) and ELN (*B*) qPCR were performed on cDNAs prepared from total RNA isolated from endothelial cells (ECs) and vascular smooth muscle cells (VSMCs) cultured separately on tissue culture plastic (5 days in 2D culture), Cultisphers laden with both ECs and VSMCs (5 days in suspension culture, 0 days in agarose molds) or individual tubular constructs (made from cellularized Cultisphers cultured in suspension culture for 5 days followed by culture for 7, 12 or 17 days in agarose molds). The plotted values show relative amounts of mRNA based on 4–6 replicate samples for each. Plotted values are standardized in relation to the reference gene, GAPDH, but similar results were obtained using TBP as a second reference gene (not shown), *Asterisks* indicate significant differences from levels in 0 days in agarose mold samples, p values <0.05.

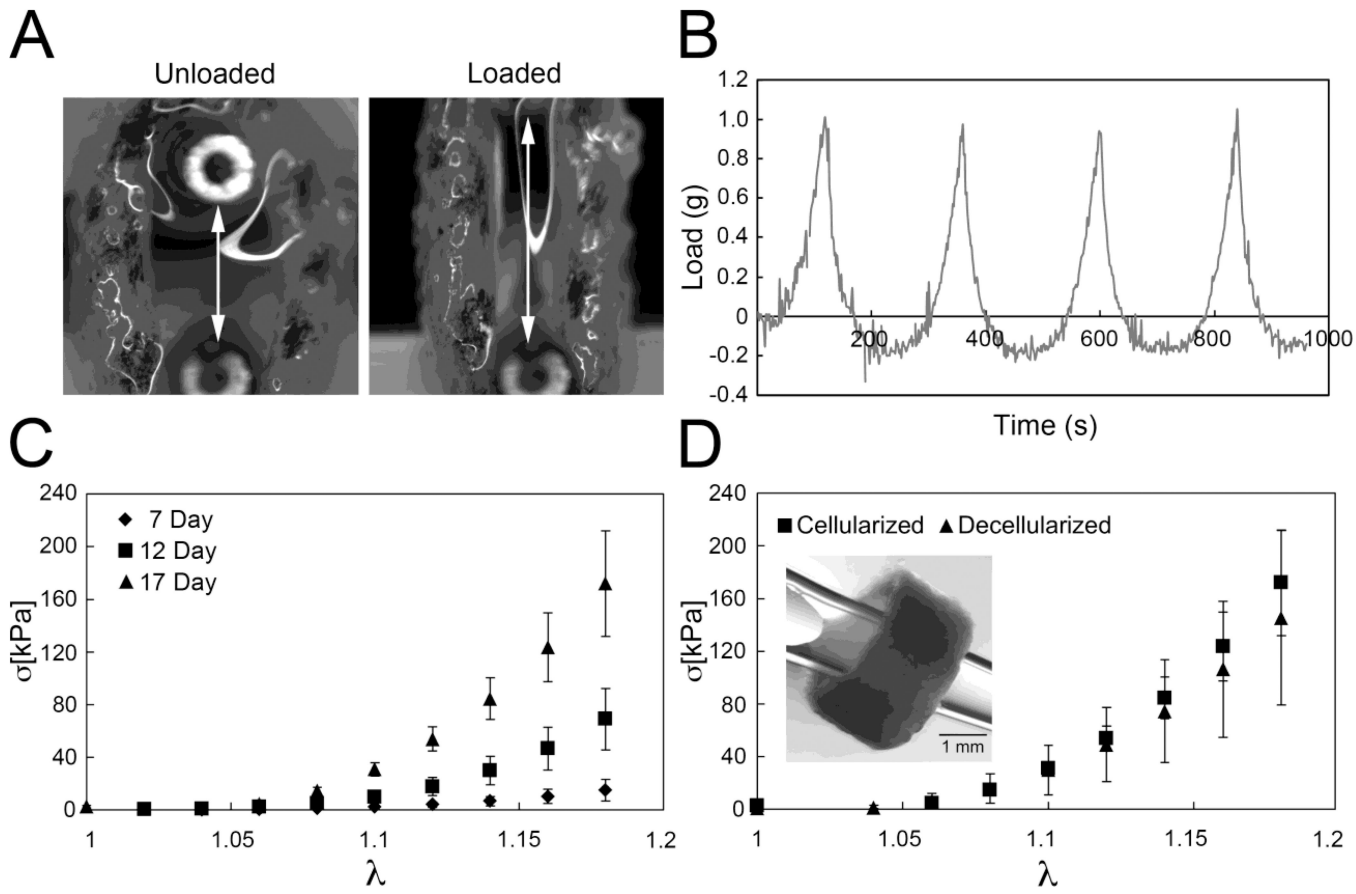

Figure 6.

Uniaxial tensile testing shows that tubular constructs exhibit a nonlinear mechanical response, *A* shows a tubular construct (cultured 7 days in an agarose mold) dyed and mounted between cannulas in an unloaded and loaded mechanical state, *B*, Load versus time curves for cyclical loading and unloading of a single construct (after 7 days in culture), *C*, Cauchy stress versus stretch ratio response of ring constructs after 7, 12, and 17 days of static culture, *D*, Cauchy stress versus stretch ratio response of tubular constructs after 17 days of static culture prior to and following decellularization, *Inset panel* in D shows a decellularized day 17 tubular construct with a pipette tip inserted through the bore, *Error bars* in *C* and *D* denote standard deviation among test samples (n=5 for cellularized constructs; n=5 for decellularized constructs).

Table 1

qPCR primer sequences

Gene	Target sequence ID no.	Forward primer 5'-3'	Reverse primer 5'-3'
ELN	NM_001081754.1/NM_001081752.1	CAGCTAAATACGGTGCTGCTG	AATCCGAAGCCAGGTCTTG
COL1A1	NM_000088.3	GGGATTCCCTGGACCTAAAG	GGAACACCTCGCTCTCCA
GAPDH	NM_002046.4	GAGTCAACGGATTTGGTCGT	GACAAGCTTCCCGTTCTCAG
TBP	NM_003194.4	CTGTATCCCTCCCCCATGAC	TGCGGTACAATCCCAGAACT